

Light-Fueled Nonreciprocal Self-Oscillators for Fluidic Transportation and Coupling

Zixuan Deng, Hang Zhang, Arri Priimagi,* and Hao Zeng*

Light-fueled self-oscillators based on soft actuating materials have triggered novel designs for small-scale robotic constructs that self-sustain their motion at non-equilibrium states and possess bioinspired autonomy and adaptive functions. However, the motions of most self-oscillators are reciprocal, which hinders their use in sophisticated biomimetic functions such as fluidic transportation. Here, an optically powered soft material strip that can perform nonreciprocal, cilia-like, self-sustained oscillation under water is reported. The actuator is made of planar-aligned liquid crystal elastomer responding to visible light. Two laser beams from orthogonal directions allow for piecewise control over the strip deformation, enabling two self-shadowing effects coupled in one single material to yield nonreciprocal strokes. The nonreciprocity, stroke pattern and handedness are connected to the fluidic pumping efficiency, which can be controlled by the excitation conditions. Autonomous microfluidic pumping in clockwise and anticlockwise directions, translocation of a micro-object by liquid propulsion, and coupling between two oscillating strips through liquid medium interaction are demonstrated. The results offer new concepts for non-equilibrium soft actuators that can perform bio-like functions under water.

1. Introduction

Stimuli-responsive materials can exhibit large shape changes in response to external energy sources such as optical^[1] and magnetic^[2] fields, heat,^[3] humidity,^[4] chemicals^[5] and so on.^[6–8] These materials have been widely used in the development of soft robots that are miniature, externally powered and compliant, triggering an emerging field of responsive-material-


based soft robotics.^[9,10] These robots often capture intriguing design principles from nature, being able to locomote,^[11–14] exhibit functions such as grasping,^[15] object recognition,^[16] and cilia-like motion.^[17–21] Conventionally, the robotic movements are determined by on-purpose field operations.^[22–24] Thus they require sophisticated design, programming, and control of the field source to achieve on-demand robotic movements.

Another nature-inspired principle arises from driving the responsive materials out of equilibrium, allowing us to realize synthetic material systems that are dynamic, autonomous, interactive and communicative.^[25] In the context of responsive-material-based soft robots, this principle can yield a radical change in the correlation between the stimulus and the response. First, the stimulus field is no more considered as a control-type operation but instead, it serves as a constant energy source to sustain the material motion without human influence.^[26–28] Second, the specific form of movement relies on the interaction between the active structure and its surrounding environment, providing the material with the ability to autonomously respond to environmental changes.^[29]

To follow the above bioinspiration scheme, the key is to attain a self-oscillating material construct that mechanically vibrates under a constant stimulus field.^[28–30] Self-sustained motions have been studied in non-equilibrium material systems driven by, for example, light,^[31] heat,^[32] and chemical reactions.^[33] The mechanisms include self-shadowing,^[34] mechanical zero-elastic-energy mode,^[35] Belousov-Zhabotinsky reaction,^[36] self-regulation between photoisomerization efficiency (change of *cis* life-time), phase transitions of the molecular assembly (crystallinity),^[37–39] etc. Based on those mechanisms, dissipative robotic systems displaying self-sustained walking, swimming, object transportation and electric power generation, have been demonstrated.^[40–44] However, the use of self-oscillating materials in microfluidics is rarely reported,^[42,45] due to the fact that most self-oscillating structures are not able to generate sufficient motions in fluids and more importantly, the typical reciprocal oscillation does not produce effective fluid-structure interaction (pumping), which highly relies on nonreciprocal strokes. Reports demonstrating a photo-deforming strips with coupled twisting and bending motions as well as travelling-wave deformation in air or solutions unveil the possibility of

material motion without human influence.^[26–28] Second, the specific form of movement relies on the interaction between the active structure and its surrounding environment, providing the material with the ability to autonomously respond to environmental changes.^[29]

Z. Deng, A. Priimagi, H. Zeng
Smart Photonic Materials
Faculty of Engineering and Natural Sciences
Tampere University
P.O. Box 541, Tampere FI 33101, Finland
E-mail: arri.priimagi@tuni.fi; hao.zeng@tuni.fi
H. Zhang
Department of Applied Physics
Aalto University
P.O. Box 15100, Espoo FI 02150, Finland

 The ORCID identification number(s) for the author(s) of this article can be found under <https://doi.org/10.1002/adma.202209683>.

© 2023 The Authors. Advanced Materials published by Wiley-VCH GmbH. This is an open access article under the terms of the Creative Commons Attribution License, which permits use, distribution and reproduction in any medium, provided the original work is properly cited.

DOI: 10.1002/adma.202209683

nonreciprocal self-oscillation.^[26,46–49] However, they do not provide a routine to program such nonreciprocity (stroke pattern) on demand. This guides us to ask the following questions: Can we obtain a light-fueled self-oscillator with programmable stroke pattern? Can we apply such motion for fluidic pumping? If yes, can it open up novel non-equilibrium functions such as interaction between two structures “communicating” through liquid medium?

Here, we address the above questions using a light-fueled liquid crystal elastomer (LCE) actuator performing self-oscillating motion under water. An optical design using two orthogonal laser beams is implemented to obtain the nonreciprocal motion with programmable stroke pattern and handedness. Autonomous fluidic pumping and coupling between two vibrating structures through fluidic interaction are demonstrated.

2. Results

To fabricate the optically-driven self-oscillating strips, we use light-responsive LCEs.^[50] Chain extension is used to oligomerize liquid crystal diacrylate monomers and primary amines via aza-Michael addition,^[51] followed by photopolymerization of remaining diacrylate end-groups to form polymer network (Figure 1a). The LCE is prepared with planar align-

ment, and thus exhibits thermally-driven contraction along the director, as shown in Figure 1b. It reaches a maximal strain of ca. 40% at 120 °C. The strain at 60 °C, that is, at temperature facilitating underwater operation, is about 10%. The LCE is then diffused with light-absorbing dye (Dispersed Red 1) to yield photothermal activation.^[52] Further details on the fabrication steps, deformability along and perpendicular to the director, mechanical properties, and absorption spectrum before and after dyeing, are given in Figures S1–S3, Supporting Information.

A 10 mm LCE strip is fixed at one end and submerged transversely in water at room temperature. The strip is excited with two laser beams from perpendicular directions, as depicted in Figure 1c. The strong absorption—88% of light energy is absorbed and converted to heat within the first 10 μm surface layer (Figure S4, Supporting Information)—together with heat dissipation in water, establishes a thermal gradient across the sample thickness, which drives the strip to bend toward the light direction. A finite-difference time-domain (FDTD) simulation (Figure S5, Supporting Information) reveals a mean temperature difference of ca. 25 °C between front (≈80 °C) and back surfaces upon 80 mW excitation for a 100 μm thick strip (Figure 1d). This temperature difference can yield 10% strain difference (Figure 1b) between the two surfaces, which is sufficient to yield efficient bending under water. The photo-induced heat distribution, and hence the photo-deformation, depends on

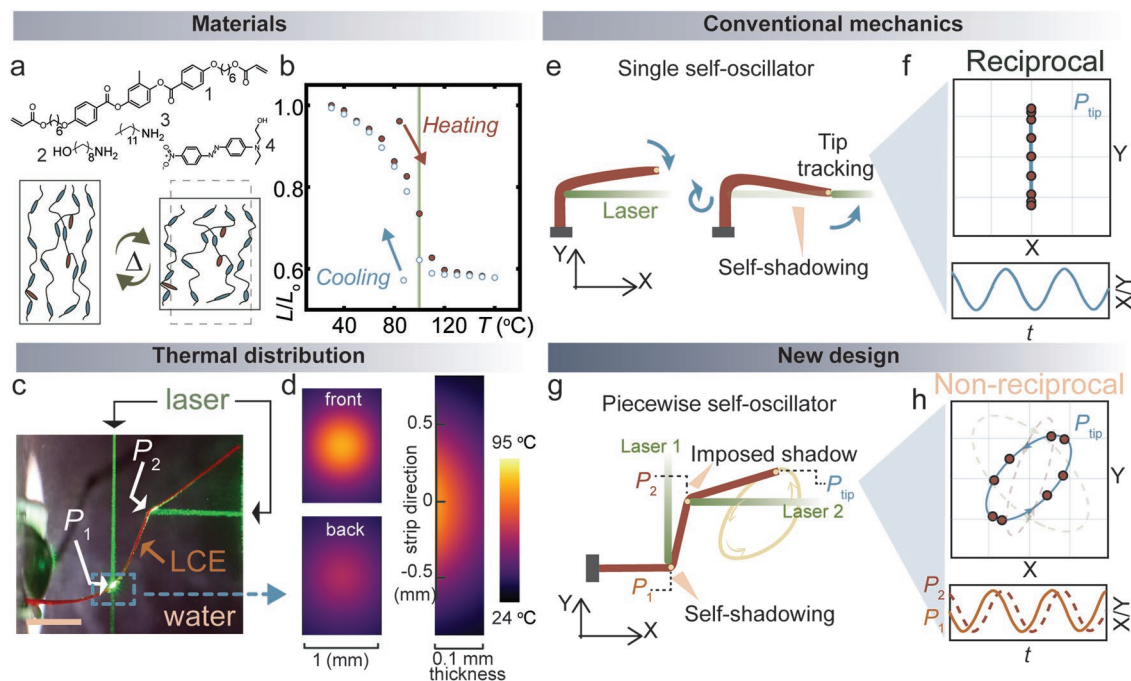


Figure 1. System concept of piecewise light-fueled self-oscillator. a) Top, compounds used for the fabrication of light-responsive liquid crystal elastomers (LCEs). 1, liquid crystal crosslinker; 2,3, chain extenders; 4, light-absorbing dye. Bottom, scheme of planar-aligned LCE experiencing anisotropic deformation upon thermal stimulus. b) Heat-induced deformation during one thermal cycle. The green bar indicates the temperature for reaching 50% of the maximal contraction. c) Photograph of LCE strip bending in response to two laser beams in water. The orthogonal laser excitation spots on the LCE are indicated as P_1 and P_2 . Laser, 532 nm, 50 mW; spot size, 1 mm. Sample thickness, 0.1 mm. Scale bar: 5 mm. d) Simulation of the photothermal distribution at the front and back surfaces of the LCE (left) and heat gradient across the sample thickness (right). Laser power: 80 mW, spot size: 1 mm. Sample thickness: 0.1 mm. e) Scheme of self-shading-induced photo-oscillation upon one-beam excitation and f) corresponding tip displacement trajectory. g) Scheme of piecewise photo-oscillator excited with two orthogonal laser beams. Laser 1 excites the bottom part of the strip and laser 2 from orthogonal direction imposes a second oscillation to the oscillating cantilever. h) Corresponding nonreciprocal stroke pattern.

the strip thickness and laser power, as detailed by simulations on thermal mapping and gradient profile in Figures S6–S8, Supporting Information. The photothermal gradient-driven actuation in a planar-aligned LCE offers two merits for programmable deformation/motion. First, the bending segment is localized at the laser spot, the position of which can be arbitrarily tuned along the strip. Second, the bending can occur toward both sides of the sample, depending on the irradiation direction.

The conventional light-fueled self-oscillation approach is based on self-shadowing, as schematically shown in Figure 1e. An LCE strip deflects in response to a light beam toward the irradiation direction. Once it bends over the beam position, the strip blocks the light from reaching the irradiation spot and shadows itself, inducing a negative feedback. After relaxation in the dark, the LCE unbends to be exposed to the beam again, and hence a new motion cycle starts. The responsive structure thus self-sustains the oscillation through one-spot deformation with one degree of freedom (DoF). Upon tracking the tip position, a linear motion pattern is obtained, as schematically shown in Figure 1f. This corresponds to reciprocal movement, which does not yield efficient fluidic interaction especially at small length scales.^[53]

The piecewise self-oscillator for obtaining nonreciprocal motion is depicted in Figure 1g. The LCE is irradiated with two laser beams simultaneously, from orthogonal directions. Laser 1 excites the bottom part of the strip (P_1 in Figure 1g), yielding the self-oscillation depicted in Figure 1f. Laser 2 excites the oscillating cantilever from an orthogonal direction, inducing another self-shadowing event at the middle part of the strip (P_2 in Figure 1g) and imposing a second oscillation. Hence two negative feedback loops are simultaneously exerted on the LCE strip, and the resultant superimposed oscillations can yield a nonreciprocal stroke as shown by the non-zero contour area of

the tip trajectory (swiping area) (Figure 1h). As will be shown, the swiping area, frequency, and handedness can be controlled by changing the excitation spot location and incident beam direction with respect to the strip position.

Combining the photothermal dynamics of the material used and the piecewise self-oscillation concept, two new possibilities are foreseen. First, the LCE strip can autonomously pump the surrounding liquid while the pumping efficiency is programmed by the nonreciprocity of the stroke pattern. Second, two individual strips may interact with each other through liquid medium, where their synchrony reflects their coupling effect. In the following, we illustrate these possibilities in detail.

Upon laser beam excitation in aqueous environment, the LCE strip bends with a deflection angle α , as shown in Figure 2a. α increases with the increase of input power, and 85° bending angle triggers sufficient shadowing for initiating the oscillation (Figure 2b). The light-induced deformation is polarization independent, as shown by the photo-induced bending angle recorded upon rotating the incident beam polarization (Figure S9, Supporting Information). We ascribe this to the fact that despite being dichroic, the samples are thick enough to absorb most of the incoming light irrespective of the polarization, therefore giving rise to similar photothermal heating in all cases. The laser-induced bending depends on the liquid temperature, and an increased temperature yields a lower power threshold for the oscillation (Figure S10, Supporting Information). The laser power used (<0.2 W) is insufficient to trigger detectable temperature changes in the water bath, due to the large volume of the liquid tank (8 cm × 8 cm × 6 cm) and sufficient heat dissipation from the tank to the environment. The mechanical properties and thickness of the LCE also affect the underwater deformability. Based on the data shown in Figure S11, Supporting Information, we select a molar ratio of 1.1:1

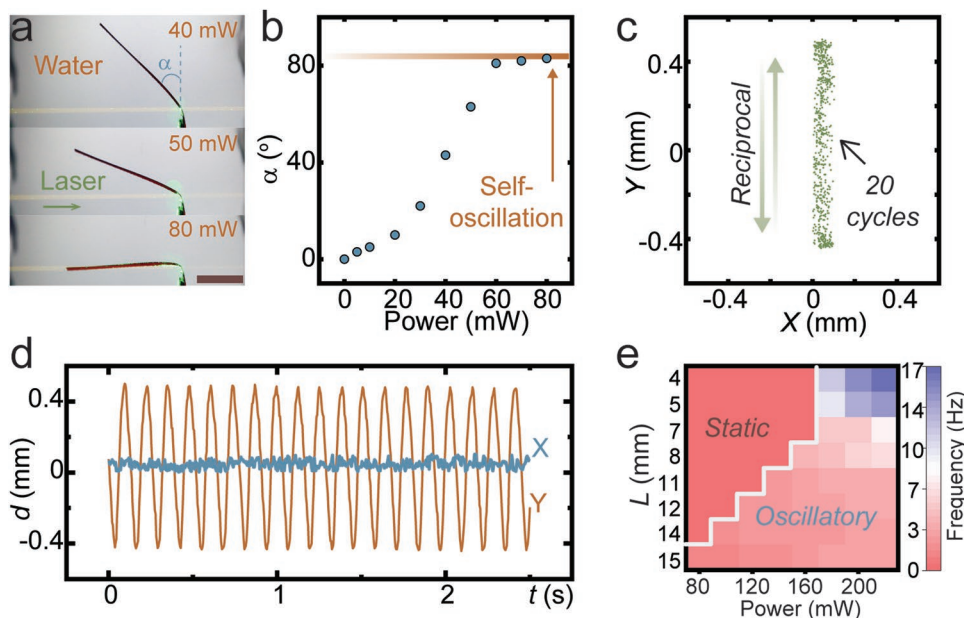


Figure 2. Single-beam-induced self-oscillation. a) Photographs of LCE strip bending in water under different excitation power. Scale bar: 5 mm. b) The bending angle α as a function of laser power. Self-oscillation requires minimum 80 mW illumination. c) X–Y trajectory of 20 oscillation cycles under single-beam excitation and d) corresponding tip displacement d in X–Y plane. Laser power: 100 mW, spot size: 1 mm. e) Color map summarizing the oscillation threshold and frequency upon different illumination power and cantilever length.

between diacrylate and amine, and 100 μm sample thickness for optimized deformability. Also the type of liquid affects the photo-deformation of the LCE strip, as exemplified by using water, silicone oil, PEG-200 and glycerol (Figure S12, Supporting Information). Self-oscillation is observed only in water, implying that medium with low enough viscosity is needed for the phenomenon to occur.

As expected, single-beam-induced self-oscillation is reciprocal, as shown by the trajectory pattern in Figure 2c. The bending motion is confined to the Y-axis direction that is perpendicular to the laser beam, governed by the shadowing orientation (Figure 2d). The power threshold strongly depends on the LCE length—the longer the strip, the less energy is needed for triggering the oscillation (Figure 2e and Movie S1, Supporting Information). Above the threshold, the oscillation frequency increases with input power, as shown in the frequency map in Figure 2e and in Figure S13, Supporting Information. Under the same excitation power, the oscillation frequency can be increased by reducing the sample dimensions (Figure S13c, Supporting Information), similar to light-driven self-oscillators previously reported in LCNs operated in air.^[34,54]

Under excitation with two orthogonal laser beams, the LCE strip bends into a zigzag configuration with clockwise deflection in one segment and anticlockwise in the other (Figure 3a). To quantify the shape change of the strip, we define the first oscillator arm, L_1 , as the distance between the laser spot P_1 close to the fixation point and the second laser spot P_2 in the middle of the strip, and the second oscillator arm L_2 as the distance between P_2 and the tip of the LCE strip P_{tip} . The actual tip motion is a result of the oscillation of arm L_2 superimposed to the oscillation of arm L_1 . The nonreciprocity is quantified as the swiping area extracted from the tip trajectory (P_{tip}) over multiple oscillation cycles, as exemplified in Figure 3b,c with two stroke patterns in X–Y plane. The length ratio between the two arms, $\delta = L_2/L_1$, greatly influences the swiping area and oscillation pattern. By increasing δ from 0.3 to 3.6, the stroke changes from a banana-like shape with a small area (1.75 mm^2) to a boat-like shape with a larger area (8.6 mm^2), as seen from Figures 3b and 3c.

The alignment of the two orthogonal beams with respect to the strip orientation determines the handedness of the oscillator. Figure 3d shows the top view of two oscillating strips with

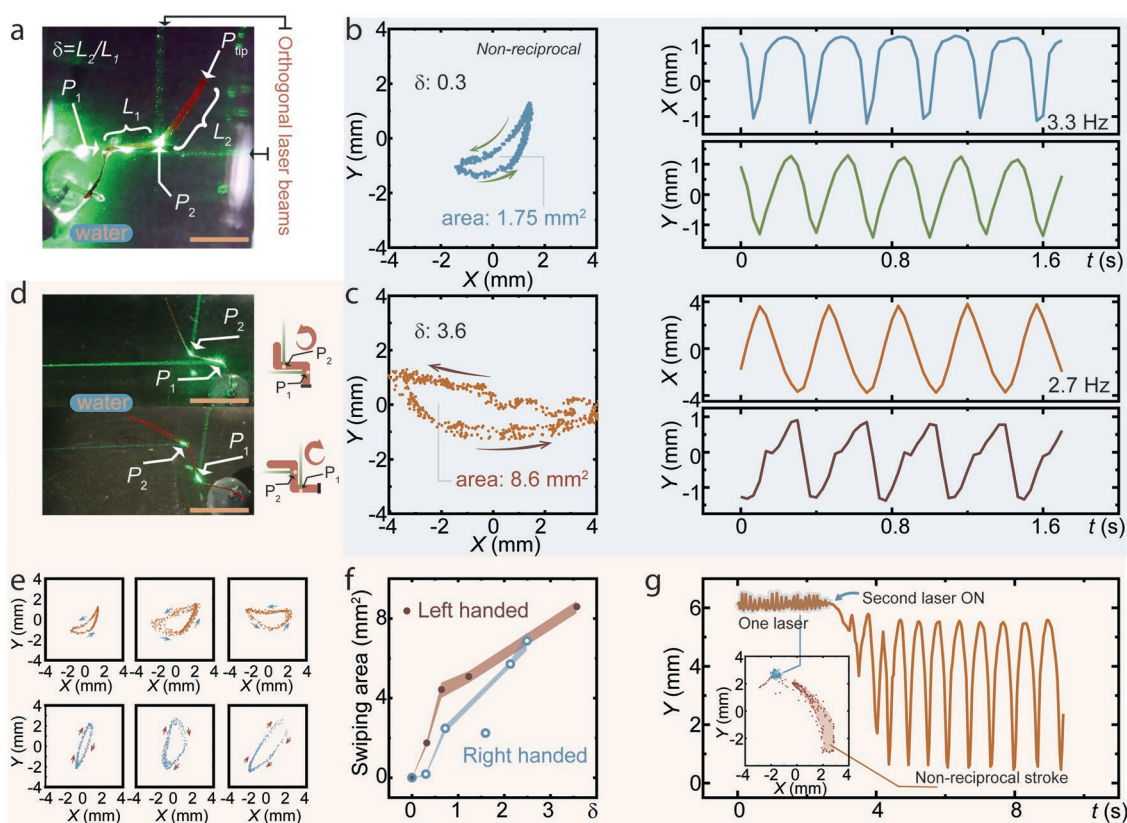


Figure 3. Piecewise self-oscillator. a) Definition of the oscillating arm ratio $\delta = L_2/L_1$, where L_1 represents the distance between first and second laser spots, L_2 represents the distance between second laser spot and the strip tip. b) X–Y trajectory for $\delta = 0.3$ with an enclosed swiping area of 1.75 mm^2 . The green arrows suggest a left-handed swiping direction. On the right: corresponding X- and Y-displacements with an oscillation frequency of 3.3 Hz. c) X–Y trajectory for $\delta = 3.6$ with an enclosed swiping area of 8.6 mm^2 . The brown arrows suggest a left-handed swiping direction. On the right: corresponding X- and Y-displacements with an oscillation frequency of 2.7 Hz. d) Photographs of two possible oscillation schemes, where the sequence of the two laser beams reaching the LCE strip determines the oscillation handedness. e) X–Y trajectories for left- (top) and right-handed (bottom) swiping. f) Swiping area versus δ for left- and right-handed swiping. g) Y-displacement evolution upon switching from single-beam-induced to two-beam-induced oscillation. Inset: corresponding X–Y trajectory. The orthogonal laser excitation spots on the LCE are indicated as P_1 and P_2 . Laser power: 100 mW, spot size: 1 mm. All scale bars: 5 mm.

different handedness. When the transverse beam hits P_1 for anticlockwise bending, and the vertical beam hits P_2 for clockwise deflection, the configuration results in left-handed self-oscillation. In turn, when the vertical beam triggers clockwise deflection and the transverse one anticlockwise, right-handed oscillation is obtained. The stroke pattern can be tuned by changing δ , as exemplified in Figure 3e for both handednesses. Further details on oscillation characterization are given in Figures S14 and S15 and Movie S2, Supporting Information. The nonreciprocity is strongly connected to δ , and the swiping area increases with an increase of δ for both left- and right-handed swiping (Figure 3f). No correlation is observed between the oscillation frequency and δ /swiping area (Figures S14f and S15f, Supporting Information). This is because the self-oscillation frequency is determined by both the delay of the material response and the resonance of the cantilever structure.^[55] In a liquid environment, interaction between the self-oscillator and the surrounding liquid adds extra complexity into the stroke movement. As a result, the oscillation characteristics deviate from conventional cilia-like devices, the frequencies of which are determined by the properties of the external fields.

Meanwhile, piecewise laser excitation allows manual switching between reciprocal (Figure 2) and nonreciprocal (Figure 3) oscillation modes, as demonstrated in Figure 3g. Upon single-beam excitation, the strip is constrained in one DoF oscillation with very limited swiping area, as indicated in the inset of Figure 3g. By turning on the second laser beam, the oscillation amplitude is significantly enhanced due to the second introduced DoF, facilitating the swiping area remarkably by a factor of 20. Further details on oscillation switching are given in Figure S16 and Movie S3, Supporting Information.

Unlike single-beam-induced self-oscillator, the piecewise oscillator endowing nonreciprocal strokes can enable practical use in microfluidic transportation as both the swiping area and handedness can be conveniently controlled. We demonstrate this with polystyrene microspheres in density-matching water:glycerol solution (4.04:1 volume ratio), using particle image velocimetry (PIV) to measure the instantaneous velocity field around the oscillating strip (Figure 4a and Figure S17, Supporting Information). The PIV snapshots unveil that the surrounding liquid is influenced by the motion of the strip, and pumped into a circling flow dictated by the stroke handedness (Figure S18 and Movie S4, Supporting Information). We divide one oscillation period into four phases, according to the movement direction in each arm, as shown by the insets of Figure 4b. It is found that the surrounding fluidic speed increases when approaching the strip surface. Vortex generation is observed around the tip position during the recovery phase, that is, at 0.34 s in Figure 4b. To quantify the pumping efficiency, we selected a linear region of interest away from the strip area, to avoid the interference of LCE strip motion and the complex vortex. The boundary is indicated by the dashed line in Figure 4b, in which a relatively stable velocity field is observed. The fluidic speed perpendicular to the boundary, v , and its position dependency at different oscillation phases, is shown in Figure 4c. v exhibits both positive and negative values at different positions across different oscillation phases, while the positive mean speed indicates a net liquid flow in the anticlockwise direction over sequential oscillation periods. The pumping

is estimated by a flux through a rectangular cross-section composed of the strip width multiplied by the length of selected line, showing a mean pumping efficiency of $0.14 \text{ cm}^3 \text{ s}^{-1}$ across the observed window (inset of Figure 4c). The pumping efficiency is closely related to δ , showing a positive correlation to the arm ratio (Figures S19 and S20, Supporting Information). The pumping efficiency and the dependency of flow on δ are similar for both left- and right-handed oscillations (Figure S21, Supporting Information).

To implement the above-described autonomous pumping in micro-object transportation, we incorporated a polystyrene polyhedron ($\approx 0.8 \text{ mm}$ side length) into the liquid. The object is propelled by the liquid flow that is induced by the right-handed oscillating strip (Figure 4d). Figure 4e shows the tracking of the object displacement along the X-axis with respect to the continuously oscillating strip, suggesting an autonomous micro-object transportation over cyclic nonreciprocal oscillation that is fueled with constant light field without human influence. Further details on object transportation are given in Figure S22 and Movie S5, Supporting Information.

The piecewise-oscillating LCE strips resemble natural cilia in a most simplified form—the underwater motion is 2D, nonreciprocal, and the motion itself is dissipative. The stroke pattern, oscillation frequency and pumping efficiency are no longer controlled by human input signal (i.e., magnitude and frequency) but originated from the interaction between the LCE strip, the light field and the surrounding liquid in an autonomous manner. Can such self-oscillating non-equilibrium strips interact with each other through the liquid medium, alike hydrodynamic coupling in natural cilia?^[56] Such communication between synthetic strips driven out of equilibrium is similar to the concept of Huygens' pendulum clock synchronization, which has been utilized to couple two polymer strips in air via mechanical interaction.^[57] In the following, we demonstrated that two LCE strips that originally exhibit different oscillating frequencies can show synchrony in pace through liquid interaction.

Figure 4f shows two right-handed self-oscillating strips separated by 5 mm distance between their fixation points. These two strips start their cyclical movements with random phases and originally exhibit 1.5 and 2.4 Hz oscillation frequencies. The asynchrony is revealed by the early-stage oscillation data in Figure 4g, showing both positive and negative phase difference between the two strips. After 13 s of oscillation, the phase difference gradually stabilizes and locks to ca. 15° . An incidental bubble (due to the local heat from the laser) appearing at 23 s disturbs the coupling, after which the phase difference quickly increases and the synchrony is lost. Another stabilization phase is reached at about 40 s, with a phase difference settled at 60° , until receiving other disturbances for desynchrony. Further details on the stroke and coupling are given in Figure S23 and Movie S6, Supporting Information.

3. Discussion

The phase locking between two nonidentical self-oscillators with frequencies f_1 and f_2 arises from the fluidic interaction between the two strips. The occurrence of synchrony (in-phase,

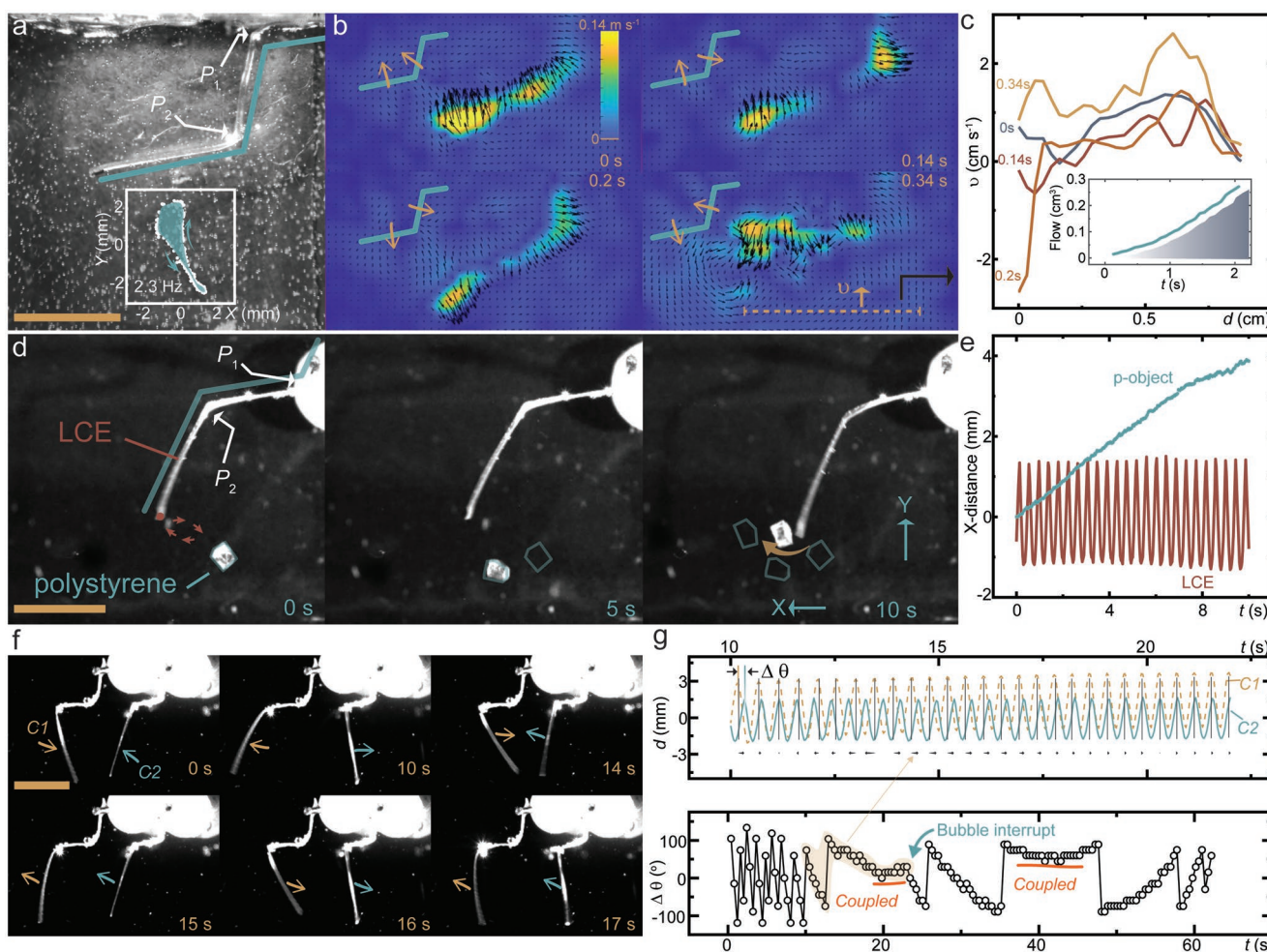


Figure 4. Pumping and coupling. a) Photograph of right-handed piecewise self-oscillator in polystyrene microsphere-dispersed fluid. Inset: X–Y trajectory with an oscillation frequency of 2.3 Hz. b) PIV images of four distinct self-oscillation phases. The color bar indicates magnitude intensity. The orange dashed line indicates the selected cross-section for flow measurement. c) Flow velocity at the selected region at different time instances. Inset: the net flow versus time. d) Images of polystyrene microparticle transportation over several self-pumping cycles. e) X-displacement of the LCE tip and the micro-object. f) Images of two neighboring strips (C1 and C2), reaching coupling via fluidic interaction. g) X-displacement of strip tips and corresponding phase difference $\Delta\theta = \theta_{C1} - \theta_{C2}$. The orthogonal laser excitation spots on the LCE are indicated as P_1 and P_2 . Laser power: 100 mW, spot size: 1 mm. All scale bars: 5 mm.

out-of-phase, constant phase delay, etc.) relies on two factors—the coupling strength and frequency detuning ($\Delta f = f_1 - f_2$). In general, the synchronization takes place when $\Delta f/F \ll 1$ (F is the coupling frequency). In practice, the mismatch between f_1 and f_2 as well as the relatively weak interaction via the fluidic medium significantly narrow the bandwidth of synchronization region, that is, the duration of coupling.^[58] In our observation, the coupling typically last for a period between 5 and 20 s, as illustrated also in Figure S24, Supporting Information. Different flow rates regulated by the active strips could be a latent reason for the different phase delay observed during the temporary coupling. Future research should tackle the technical hurdles to realize more complex coupling behavior in a controllable manner.

Based on the PIV analysis for fluidic pumping, we deduce the Reynolds number $Re = \frac{\rho L^2 f}{\mu} = 60$, where the active strip length, $L = L_2 = 7$ mm, the oscillating frequency (f), fluid dynamic vis-

cosity (μ) and density (ρ) at 22 °C are 2.3 Hz, 0.002 Pa s and 1.056 g cm⁻³, respectively. The Reynolds number value suggests a laminar flow, where both inertial forces and viscous drag govern the motion of the strip. The oscillation coupling between two strips in water does not appear to be in-phase or anti-phase, which are the cases often observed in mechanical systems, as well as natural coupled cilia.^[56] The phase difference between the adjacent strips can induce a net flow, and this is the strategy natural cilia uses to produce metachronal waves for liquid transportation.^[59] Varied phase differences correspond to different net flow that has been stabilized between the structures. There are two phase differences observed in our strips, 15° at 20 s and 60° at 40 s. We speculate that different flow rates may be regulated by the active strips along the oscillating period.

The alignment of the incident beams is critical, since out-of-plane excitation may lead to nonreciprocal oscillation with an analemma figure with both handednesses (Figure S25,

Supporting Information). The design principle of the piecewise nonreciprocal self-oscillator could be applicable also to other responsive material systems such as hydrogels. However, particular attention should be paid to the material deformability under water. The chain-extended LCEs used in this study, alike conventional glassy liquid crystal networks, can both exhibit self-oscillation in air (Figures S26 and S28, Supporting Information). However, the latter fails in performing self-oscillation under water due to its limited deformability and higher photothermal temperature required for deformation (Figure S27, Supporting Information). The pumping efficiency and coupling capacity are significantly influenced by the specific stroke pattern in each oscillating strip. To first demonstrate the principle, we have adopted an identical laser power (100 mW) between two orthogonal beams for excitation. Future research may include the change of laser powers and the two spot positions in parallel, in order to obtain a more sophisticated tunability in stroke pattern and oscillation frequency.

Conventional artificial cilia devices are controlled through periodic modulation of magnetic field to endow nonreciprocal movement inside liquids.^[18,60] However, these cilia-like motions are fundamentally different from their biological counterparts. First, magnetically-driven cilia are forced to deform by the external field, thus, the entire operation principle of magneto-cilia is well in-phase with an external control signal, and the pumping behavior is not regulated by interaction between the structure and the surrounding environment. Second, the phase differences in magneto-cilia are determined by the material response encoded during the magnetization process and cannot be tuned post the fabrication.^[18,61] Typical field-driven cilia devices are performed under human control and manipulation, but not functionalized autonomously at a non-equilibrium state. Conversely, the light-fueled nonreciprocal self-oscillators function out of equilibrium and exhibit tunable strokes, and the fluidic pumping and coupling are rooted in the interaction between the active material and the surrounding liquid. It serves as a novel experimental model of dissipative material motor, simplistically mimicking natural systems. Hence, we believe that our results can provide a new perspective to the design of actuators with life-like functions.

Photochemically induced deformation in LCEs has many significant merits such as isothermal and in some cases bistable actuation. However, for micro-robotics, the photothermal mechanism offers an advantage of high-speed for shape morphing. The photothermal actuation speed is governed by the speed of the heating-cooling cycle, and thus is determined by the heat capacity of the material. Downscaling the size results in a decreased heat capacity, accelerated heat dissipation, and enhanced actuation speed. Figure S29, Supporting Information, shows the oscillation data of a miniaturized strip with a length of 2 mm, for which the self-oscillation frequency reaches 54 Hz as compared to 3 Hz for a 15 mm long strip. Switching the light source periodically on and off, the frequency can be as high as 100 Hz. Nonreciprocal oscillation and significantly enhanced swiping area by a factor of 16 can also be induced in the miniaturized strip by using two modulated laser beams, as explicated in Figure S30, Supporting Information. Upon further downscaling the structure size, two-photon absorption

laser fabrication can be used, as has been successfully proven for micron-sized LCE elements with sub-millisecond actuation speed.^[62] The challenge foreseen for integration of multiple coupled micro-scale LCE strips is the complex arrangement of orthogonal laser beams and excitation spot positions with respect to each actuator. Micro-fabricated waveguides, providing precise excitation and multi-unit connections, can be one possible solution for this.

The drawback of using photothermal mechanism for underwater actuation is the convection that local heating may generate. In our experiments, we adopt a configuration in which we follow the movements of the LCE strip in the horizontal X–Y plane, while the convection flow mainly affects the velocity in the vertical (Z) direction. Figure S31, Supporting Information, elaborates the PIV measurement of the photothermally induced convection while ceasing the self-oscillation by mechanical fixation of the LCE strip. The data shows a flow of few centimeters per second along the vertical direction but negligible velocity component along the strip direction. This experimental configuration allows basic study of liquid pumping and coupling on the sample plane, minimizing the influence of convection. Future studies may include using LCEs with lower phase transition temperature,^[63] to suppress the heat-induced convection.

The contemporary trends in soft robotics are to go to small scale, adapt to complex environment, and obtain decentralized control over the robotic motions. All these trends require new materials to be implemented.^[64] A biologically inspired robotic material should be able to sense, actuate, self-control and interact with the environment, but without the need of bulky electronics and complex computing.^[25] This vision requires future robotic materials to be increasingly “life-like” and one of the most important principles behind “life-like” materials is that they should function out of equilibrium, allowing to realize synthetic material systems that are dynamic, autonomous, interactive and communicative.

4. Conclusion

In summary, we report an orthogonal laser excitation approach to obtain nonreciprocal, underwater self-oscillation in soft matter. The soft actuator is made of light-responsive LCE strip that is excited piecewise with two constant laser beams for attaining programmable stroke patterns under water. We demonstrate autonomous fluidic pumping, micro-object transportation, and coupling between two strips through fluidic interaction. We would like to emphasize the following features in this self-oscillating system. First, the nonreciprocal oscillating strips function out of equilibrium, that is, the system can be deemed as dissipative, resembling living organisms. Second, the stroke frequency and pumping behavior are dictated by interaction between the self-oscillator and the surrounding liquid, while the light beam position provides opportunity to tune and program the stroke patterns. Third, it allows interaction between different strips through the liquid medium. We wish our results can bring novel design of stimuli-responsive soft robots that possess bio-like function at their non-equilibrium states.

5. Experimental Section

Materials in Brief: 1,4-Bis-[4-(6-acryloyloxyhexyloxy)benzoyloxy]-2-methylbenzene (99%, RM82) was obtained from SYNTHON Chemicals. 8-amino-1-octanol and dodecylamine were obtained from TCI. 2,2-Dimethoxy-2-phenylacetophenone and glycerol solution (86–89%) were obtained from Sigma-Aldrich. Disperse Red 1 was obtained from Merck. Polystyrene microspheres ($97.1 \pm 1.7 \mu\text{m}$) were obtained from Thermo Fischer Scientific. All chemicals were used as received.

Sample Fabrication: Liquid crystal cells were prepared by gluing two functionalized glass substrates, both with rubbed polyvinyl alcohol (PVA, 5 wt% water solution, 4000 RPM, 1 min, baked at 100°C for 10 min) for uniaxial alignment. $100 \mu\text{m}$ microspheres (Thermo scientific) were used as spacers to determine the film thickness. The liquid crystal mixture was prepared by mixing 0.22 mmol RM82, 0.1 mmol 8-amino-1-octanol, 0.1 mmol dodecylamine, and 2.5 wt% of 2,2-dimethoxy-2-phenylacetophenone at 85°C . The mixture was filled into the cell via capillary force at 85°C and maintained for 10 min before cooling down to 63°C (1°C min^{-1}). The cell was kept in the oven for 24 h at 63°C to allow aza-Michael addition reaction for oligomerization. Then the sample was irradiated with UV light (365 nm , 180 mW cm^{-2} , 30 min) for polymerization. Finally, the cell was opened by a blade, followed by immersion in Disperse Red 1-isopropanol solution for dyeing before strips were cut from the film.

Optical Characterization: Photographs and movies of single-beam-excited oscillator were captured with Canon 5D Mark III camera with 100 mm lens. Photographs and movies of piecewise oscillator were recorded with Edmund Optics monochrome Camera (EO-6412M), equipped with a Navitar macro lens. A continuous laser (532 nm , 2 W , ROITHNER) was used for light excitation.

Data Analysis: The movement was recorded and quantitative data were extracted from the movie with a video analysis software (Tracker). The fluid field evolution was analyzed with PIV software in Matlab.^[65]

Simulation: For the COMSOL numerical simulation, a Heat Transfer module had been coupled with a Radiative Beam in Absorbing Media module. A rectangular LCE ribbon was placed inside an aqueous environment with geometries and boundaries conditions specified in Figure S5, Supporting Information, with LCE assuming a heat capacity of $1200 \text{ J kg}^{-1} \text{ K}^{-1}$, density of 1200 kg m^{-3} , and thermal conductivity of $2.0 \text{ W m}^{-1} \text{ K}^{-1}$. The absorption coefficient of the LCE was $212\,000 \text{ m}^{-1}$, as determined by the UV–Vis spectroscopy (Figure S4, Supporting Information). The beam assumes a built-in Gaussian profile with a standard deviation of 0.263 mm . Stationary Study was used to acquire the temperature profile at equilibrium.

Supporting Information

Supporting Information is available from the Wiley Online Library or from the author.

Acknowledgements

The authors acknowledge funding from Academy of Finland (Postdoctoral Researcher No. 331015 to H.Zh., Research Fellow No. 340263 to H.Ze., Center of Excellence in Life-Inspired Hybrid Materials, LIBER, No. 346107 and the Flagship Programme on Photonics Research and Innovation, PREIN, No. 320165 to A.P.). Z.D. is supported by European Union's Horizon 2020 Research and Innovation Programme under the Marie Skłodowska-Curie Grant Agreement No. 956150 (STORM-BOTS). The authors thank Matilda Backholm (Aalto University) for the insightful discussion.

Conflict of Interest

The authors declare no conflict of interest.

Data Availability Statement

The data that support the findings of this study are available from the corresponding author upon reasonable request.

Keywords

artificial cilia, liquid crystal elastomer, micro-robots, nonreciprocal motion, photoactuator, self-sustained oscillation

Received: October 20, 2022

Revised: November 30, 2022

Published online:

- [1] J. A. Lv, Y. Liu, J. Wei, E. Chen, L. Qin, Y. Yu, *Nature* **2016**, 537, 179.
- [2] W. Hu, G. Z. Lum, M. Mastrangeli, M. Sitti, *Nature* **2018**, 554, 81.
- [3] Y. S. Kim, M. Liu, Y. Ishida, Y. Ebina, M. Osada, T. Sasaki, T. Hikima, M. Takata, T. Aida, *Nat. Mater.* **2015**, 14, 1002.
- [4] H. Arazoe, D. Miyajima, K. Akaike, F. Araoka, E. Sato, T. Hikima, M. Kawamoto, T. Aida, *Nat. Mater.* **2016**, 15, 1084.
- [5] E. Mattia, S. Otto, *Nat. Nanotechnol.* **2015**, 10, 111.
- [6] A. S. Gladman, E. A. Matsumoto, R. G. Nuzzo, L. Mahadevan, J. A. Lewis, *Nat. Mater.* **2016**, 15, 413.
- [7] T. Matsuda, R. Kawakami, R. Namba, T. Nakajima, J. P. Gong, *Science* **2019**, 363, 504.
- [8] E. Siéfert, E. Reyssat, J. Bico, B. Roman, *Nat. Mater.* **2019**, 18, 24.
- [9] L. Hines, K. Petersen, G. Z. Lum, M. Sitti, *Adv. Mater.* **2017**, 29, 1603483.
- [10] S. I. Rich, R. J. Wood, C. Majidi, *Nat. Electron.* **2018**, 1, 102.
- [11] Y. Kim, J. Van Den Berg, A. J. Crosby, *Nat. Mater.* **2021**, 20, 1695.
- [12] H. Guo, A. Priimagi, H. Zeng, *Adv. Funct. Mater.* **2022**, 32, 2108919.
- [13] S. Palagi, A. G. Mark, S. Y. Reigh, K. Melde, T. Qiu, H. Zeng, C. Parmeggiani, D. Martella, A. Sanchez-Castillo, N. Kapernaum, F. Giesselmann, D. S. Wiersma, E. Lauga, P. Fischer, *Nat. Mater.* **2016**, 15, 647.
- [14] Y. Chen, H. Zhao, J. Mao, P. Chirarattananon, E. F. Helbling, N. s. P. Hyun, D. R. Clarke, R. J. Wood, *Nature* **2019**, 575, 324.
- [15] M. P. da Cunha, H. S. Kandail, J. M. J. den Toonder, A. P. H. J. Schenning, *Proc. Natl. Acad. Sci. USA* **2020**, 117, 17571.
- [16] O. M. Wani, H. Zeng, A. Priimagi, *Nat. Commun.* **2017**, 8, 15546.
- [17] E. Milana, R. Zhang, M. R. Vetrano, S. Peerlinck, M. de Volder, P. R. Onck, D. Reynaerts, B. Gorissen, *Sci. Adv.* **2020**, 6, eabd2508.
- [18] H. Gu, Q. Boehler, H. Cui, E. Secchi, G. Savorana, C. De Marco, S. Gervasoni, Q. Peyron, T.-Y. Huang, S. Pane, A. M. Hirt, D. Ahmed, B. J. Nelson, *Nat. Commun.* **2020**, 11, 2637.
- [19] S. Li, M. M. Lerch, J. T. Waters, B. Deng, R. S. Martens, Y. Yao, D. Y. Kim, K. Bertoldi, A. Grinthal, A. C. Balazs, J. Aizenberg, *Nature* **2022**, 605, 76.
- [20] H. Zhang, L. Koens, E. Lauga, A. Mourran, M. H. Möller Zhang, A. Mourran, M. Möller, L. Koens, E. Lauga, *Small* **2019**, 15, 1903379.
- [21] W. Wang, Q. Liu, I. Tanasijevic, M. F. Reynolds, A. J. Cortese, M. Z. Miskin, M. C. Cao, D. A. Muller, A. C. Molnar, E. Lauga, P. L. McEuen, I. Cohen, *Nature* **2022**, 605, 681.
- [22] R. Di Leonardo, A. Búzás, L. Kelemen, G. Vizsnyiczai, L. Oroszi, P. Ormos, *Phys. Rev. Lett.* **2012**, 109, 034104.
- [23] H. Kim, S. Sundaram, J. H. Kang, N. Tanjeem, T. Emrick, R. C. Hayward, *Proc. Natl. Acad. Sci. USA* **2021**, 118, e2024581118.
- [24] F. Ji, D. Jin, B. Wang, L. Zhang, *ACS Nano* **2020**, 14, 6990.
- [25] C. Kaspar, B. J. Ravoo, W. G. Van Der Wiel, S. V. Wegner, W. H. P. Pernice, *Nature* **2021**, 594, 345.
- [26] A. H. Gelebart, D. J. Mulder, M. Varga, A. Konya, G. Vantomme, E. W. Meijer, R. L. B. Selinger, D. J. Broer, *Nature* **2017**, 546, 632.

- [27] X. He, M. Aizenberg, O. Kuksenok, L. D. Zarzar, A. Shastri, A. C. Balazs, J. Aizenberg, *Nature* **2012**, 487, 214.
- [28] R. K. Manna, A. Laskar, O. E. Shklyae, A. C. Balazs, *Nat Rev Phys* **2021**, 4, 125.
- [29] Y. Kageyama, *ChemPhotoChem* **2019**, 3, 327.
- [30] A. Jenkins, *Phys. Rep.* **2013**, 525, 167.
- [31] A. S. Kuentler, Y. Chen, P. Bui, H. Kim, A. DeSimone, L. Jin, R. C. Hayward, *Adv. Mater.* **2020**, 32, 2000609.
- [32] X.-Q. Wang, C. Fu Tan, K. H. Chan, X. Lu, L. Zhu, S.-W. Kim, G. W. Ho, *Nat. Commun.* **2018**, 9, 3438.
- [33] E. Nakouzi, O. Steinbock, *Sci. Adv.* **2016**, 2, e160114.
- [34] A. H. Gelebart, G. Vantomme, E. W. Meijer, D. J. Broer, *Adv. Mater.* **2017**, 29, 1606712.
- [35] A. Baumann, A. Sánchez-Ferrer, L. Jacomine, P. Martinoty, V. Le Houerou, F. Ziebert, I. M. Kulić, *Nat. Mater.* **2018**, 17, 523.
- [36] S. Maeda, Y. Hara, T. Sakai, R. Yoshida, S. Hashimoto, *Adv. Mater.* **2007**, 19, 3480.
- [37] T. Ikegami, Y. Kageyama, K. Obara, S. Takeda, *Angew. Chem., Int. Ed.* **2016**, 128, 8379.
- [38] K. Obara, Y. Kageyama, S. Takeda, *Small* **2022**, 18, 2105302.
- [39] F. Ong, D. Kitagawa, I. Bushnak, R. O. Al-Kaysi, C. J. Bardeen, *Angew. Chem., Int. Ed.* **2021**, 60, 2414.
- [40] Y. Hu, Q. Ji, M. Huang, L. Chang, C. Zhang, G. Uan Wu, B. Zi, N. Bao, W. Hen, Y. Wu, *Angew. Chem., Int. Ed.* **2021**, 60, 20511.
- [41] J. J. Wie, M. R. Shankar, T. J. White, *Nat. Commun.* **2016**, 7, 13260.
- [42] Y. Zhao, C. Xuan, X. Qian, Y. Alsaïd, M. Hua, L. Jin, X. He, *Sci. Robot.* **2019**, 4, eaax7112.
- [43] Y. Shiraki, R. Yoshida, *Angew. Chem., Int. Ed.* **2012**, 124, 6216.
- [44] L. Yang, L. Chang, Y. Hu, M. Huang, Q. Ji, P. Lu, J. Liu, W. Chen, Y. Wu, *Adv. Funct. Mater.* **2020**, 30, 1908842.
- [45] Z. Li, N. V. Myung, Y. Yin, *Sci. Robot.* **2021**, 6, 4523.
- [46] M. Hua, C. Kim, Y. Du, D. Wu, R. Bai, X. He, *Matter* **2021**, 4, 1029.
- [47] F. Ge, R. Yang, X. Tong, F. Camerel, Y. Zhao, *Angew. Chem., Int. Ed.* **2018**, 130, 11932.
- [48] T. Zhao, Y. Fan, J. A. Lv, *ACS Appl. Mater. Interfaces* **2022**, 14, 23839.
- [49] J. Wang, B. Yang, M. Yu, H. Yu, *ACS Appl. Mater. Interfaces* **2022**, 14, 15632.
- [50] T. H. Ware, M. E. McConney, J. J. Wie, V. P. Tondiglia, T. J. White, *Science* **2015**, 347, 982.
- [51] H.-H. Yoon, D.-Y. Kim, K.-U. Jeong, S.-K. Ahn, *Macromolecules* **2018**, 51, 1141.
- [52] M. Cheng, H. Zeng, Y. Li, J. Liu, D. Luo, A. Priimagi, Y. J. Liu, *Adv. Sci.* **2021**, 9, 2103090.
- [53] E. M. Purcell, *Am. J. Phys.* **1977**, 45, 3.
- [54] T. J. White, N. V. Tabiryan, S. V. Serak, U. A. Hrozhyk, V. P. Tondiglia, H. Koerner, R. A. Vaia, T. J. Bunning, *Soft Matter* **2008**, 4, 1796.
- [55] H. Zeng, M. Lahikainen, L. Liu, Z. Ahmed, O. M. Wani, M. Wang, H. Yang, A. Priimagi, *Nat. Commun.* **2019**, 10, 5057.
- [56] W. Gilpin, M. S. Bull, M. Prakash, *Nat. Rev. Phys.* **2020**, 2, 74.
- [57] G. Vantomme, L. C. M. Elands, A. H. Gelebart, E. W. Meijer, A. Y. Pogromsky, H. Nijmeijer, D. J. Broer, *Nat. Mater.* **2021**, 20, 1702.
- [58] Pikovsky Arkady, Rosenblum Michael, Kurths Jürgen, *Synchronization: A Universal Concept in Nonlinear Sciences*, Cambridge University Press, New York **2001**.
- [59] M. A. Sleigh, J. R. Blake, N. Liron, *Am. Rev. Respir. Dis.* **1988**, 137, 726.
- [60] M. Vilfan, A. Potočnik, B. Kavčič, N. Osterman, I. Poberaj, A. Vilfan, D. Babič, *Proc. Natl. Acad. Sci. USA* **2010**, 107, 1844.
- [61] X. Dong, G. Z. Lum, W. Hu, R. Zhang, Z. Ren, P. R. Onck, M. Sitti, *Sci. Adv.* **2020**, 6, eabc9323.
- [62] S. Nocentini, D. Martella, C. Parmeggiani, S. Zanotto, D. S. Wiersma, *Adv. Opt. Mater.* **2018**, 6, 1800167.
- [63] G. E. Bauman, J. M. McCracken, T. J. White, *Angew. Chem., Int. Ed.* **2022**, 61, e202202577.
- [64] P. Fratzl, M. Friedman, K. Krauthausen, W. Schäffner, *Active Materials*, De Gruyter, Berlin, Boston **2022**.
- [65] W. Thielicke, R. Sonntag, *J. Open Res. Software* **2021**, 9, 12.